



Full Length Article

Simultaneous measurement of X-ray scattering and photoluminescence during molecular deposition

N. Mrkyvkova^{a,b,*}, V. Held^a, Y. Halahovets^a, P. Nádaždy^{a,c}, M. Jergel^{a,b}, E. Majková^{a,b}, F. Schreiber^d, P. Siffalovic^{a,b}

^a Institute of Physics, Slovak Academy of Sciences, Dúbravská cesta 9, 845 11, Bratislava, Slovakia

^b Center for Advanced Materials Application, Slovak Academy of Sciences, Dúbravská cesta 9, 845 11, Bratislava, Slovakia

^c Institute of Electrical Engineering, Slovak Academy of Sciences, Dúbravská cesta 9, 845 11, Bratislava, Slovakia

^d Institute of Applied Physics, University of Tübingen, Auf der Morgenstelle 10, 72076, Tübingen, Germany



ARTICLE INFO

Keywords:

In situ photoluminescence
X-ray scattering
Molecular orientation
Organic thin-film
Vacuum deposition

ABSTRACT

We present a simultaneous *in situ* measurement of X-ray scattering and photoluminescence (PL) spectroscopy during organic thin-film growth in a vacuum. We have designed a modified deposition chamber that broadens its utilization and enables complementary information on the structure and optoelectronic properties. In a pilot experiment, we investigated the growth of diindenoperylene (DIP) thin films in real time. We found a direct correlation between PL and grazing-incidence wide-angle X-ray scattering (GIWAXS), showing the formation of a new DIP polymorph starting at a layer thickness of ~14 nm. Furthermore, we show that the PL signal is more sensitive to the arrangement of the molecules than GIWAXS in the limit of small layer thicknesses. The presented experimental setup paves the way for performing simultaneous PL and X-ray scattering measurements during the growth of various materials suitable for optoelectronic applications.

1. Introduction

Conjugated organic polymers and small molecules attract considerable interest due to their increasing use in key (opto)electronic applications such as transistors, light-emitting devices, or solar cells [1–6]. In addition, some of their unique properties, e.g., the mechanical flexibility, easy functional modification, and adjustment of the functional properties via structure, favor them over inorganic materials. Frequently, the growth of highly oriented crystalline films is required for efficient performance in organic-based devices. Therefore, it is essential to understand the growth details – from the nucleation phase to the formation of the thin/thick film – to exploit this knowledge for controlled molecular assembly and orientation. The growth of crystalline organic layers is a tremendously broad topic, covering a variety of crystal shapes and phases, molecular spatial arrangement, and surface roughness. All these factors determine the electronic and optical performance of the potential device. At the same time, understanding the structure formation of the systems is also a formidable fundamental challenge [7–10]. Therefore, *in situ* monitoring of the organic layer formation in real time is highly desirable. Typically, either the structural

or optical properties are investigated during the material growth, followed by a plethora of further *ex-situ* characterization [9,11–13]. However, simultaneous investigation of structural and optical properties brings many advantages and broadens the knowledge about material evolution and transformation in terms of the fundamental coupling of the electronic and structural properties.

X-ray scattering is a well-known experimental tool that is extensively used to characterize the structural properties of thin organic films. In particular, the grazing-incidence wide- and small-angle X-ray scattering (GIWAXS/GISAXS) provide complex information about the thin-film structure, morphology, and molecular orientation [14–16]. On the other hand, optical techniques such as absorption and photoluminescence (PL), in particular, give information about defects, electronic interactions, exciton states and lifetimes, and molecular organization [17–20].

This paper presents a combined study of structural and optical properties during the deposition of organic thin films. A specially designed deposition chamber is employed, allowing simultaneous measurement of X-ray scattering and PL during molecular growth. We have chosen diindenoperylene (DIP, C₃₂H₁₆) as an extensively studied

* Corresponding author. Institute of Physics, Slovak Academy of Sciences, Dúbravská cesta 9, 845 11, Bratislava, Slovakia.

E-mail address: nada.mrkyvkova@savba.sk (N. Mrkyvkova).

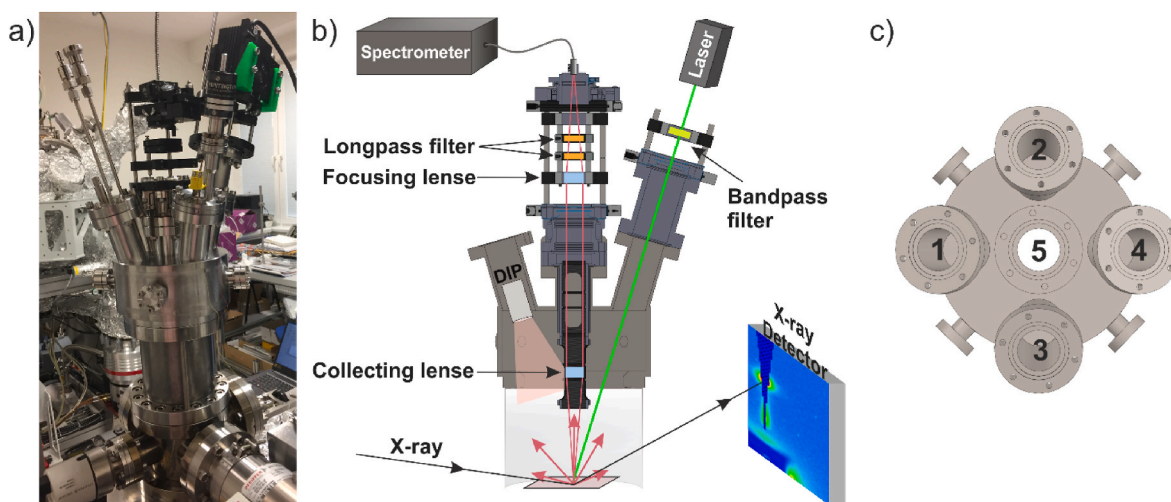


Fig. 1. a) Photograph of the custom-built deposition chamber for simultaneous *in situ* X-ray diffraction and photoluminescence measurements. b) Schematic drawing of the deposition chamber and the experimental setup. c) Top view of the deposition chamber top with the ports numbered following the description in the main text.

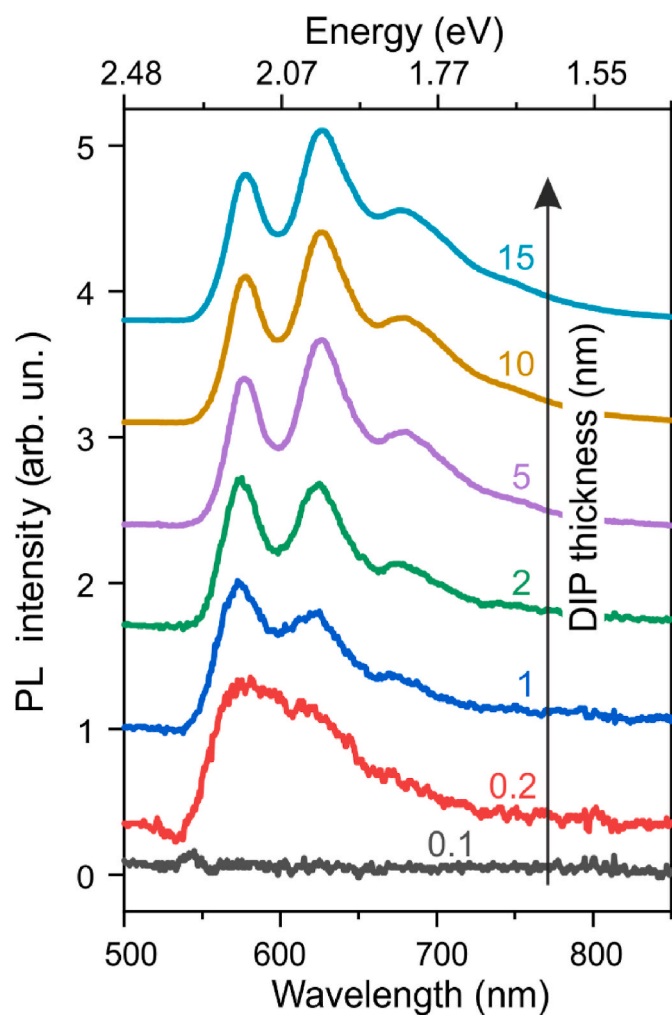


Fig. 2. Normalized PL spectra of DIP layers with different effective thicknesses (0.1–15 nm) grown on native Si substrate. A black arrow indicates DIP layer thickness increase. The spectra are offset for better clarity.

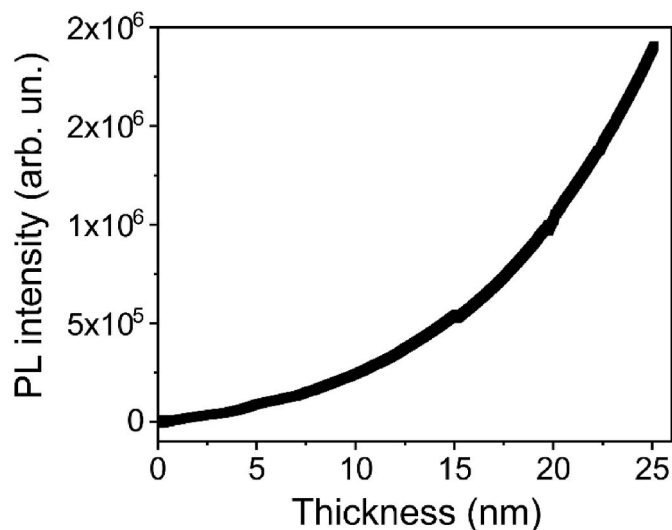


Fig. 3. Thickness dependence of the spectrally integrated PL intensity.

representative of the π -conjugated molecules. DIP and its derivatives are known to be well-absorbing donor materials with relatively high carrier mobility, exhibiting an extraordinarily high structural order on silicon dioxide [21–23].

We show that the PL spectra of DIP exhibit non-interacting molecular interaction at the beginning of growth, continually progressing to a condensed system and gradually red-shifting the spectral features. Furthermore, the PL spectral intensity was correlated with the GIWAXS diffraction pattern, indicating the existence of a polymorph with a changed molecular orientation from the layer thickness greater than 14 nm. Finally, by analyzing molecular growth *in situ*, we show that simultaneous measurement of X-ray scattering and PL spectra is of great advantage for various materials where optoelectronic and structural properties need to be correlated during vapor deposition.

2. Experimental

Fig. 1 schematically shows the vacuum chamber for organic molecular beam deposition (OMBD), with the original design similar to the one employed by Ritley et al. [24], enabling simultaneous measurement of X-ray scattering and PL during growth. The deposition chamber is

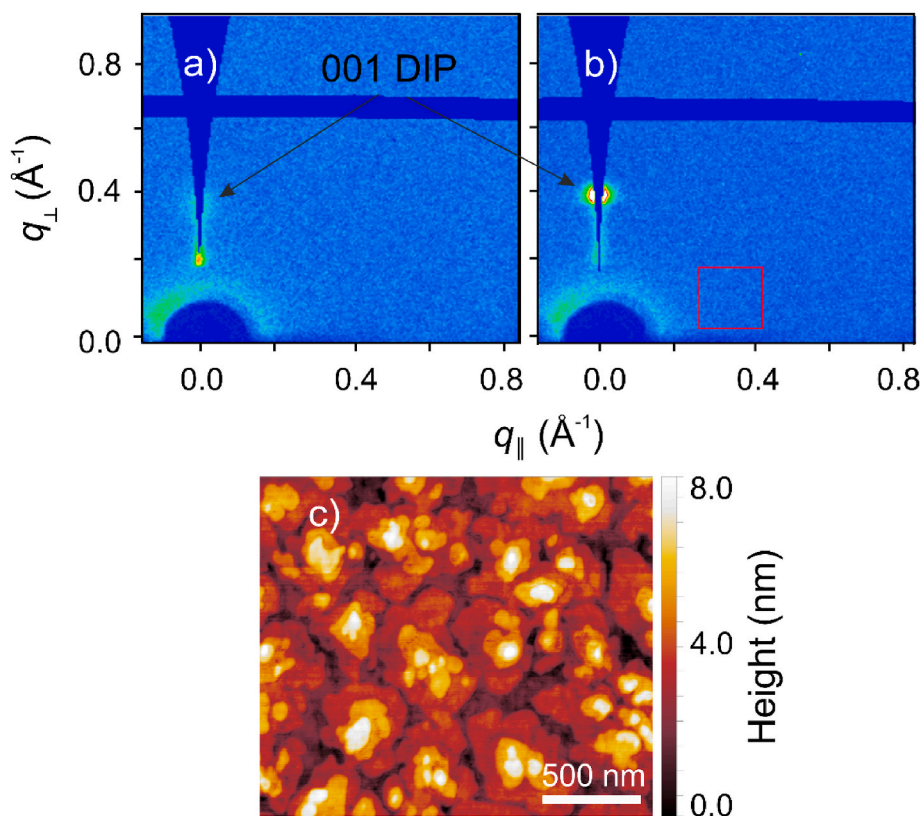


Fig. 4. Two-dimensional reciprocal space maps measured in the GIWAXS geometry for a) 5 nm and b) 25 nm thick DIP film on native Si substrate. The GIWAXS intensity increases from blue to white. The arrows indicate the 001 diffractions, and the red square indicates a predicted position of the 001 diffraction for the lying-down orientation of DIP molecules. c) AFM image of the DIP crystals. (For interpretation of the references to colour in this figure legend, the reader is referred to the Web version of this article.)

equipped with a 360° cylindrical beryllium window that allows a variety of X-ray scattering experiments. The upper hemispherical section comprises five DN40FC ports one of them being placed right above the sample and the other four equidistantly positioned in the corners of the square around it (see Fig. 1c). As shown in Fig. 1b and c, the DIP evaporator (Knudsen-style effusion cells) was placed in one of the off-centered ports (1). We note that the ports at the chamber top are numbered from (1) to (5), as indicated in Fig. 1c. A calibrated quartz crystal for monitoring the thickness of the deposited material was placed in port (2). An optical window was placed in the third off-centered port (3) to allow visual inspection of the sample surface before/after the deposition. The last off-centered port (4) was occupied with an excitation laser ($\lambda = 532$ nm, Lasever). The laser excitation energy is well above the transition energy from the lowest vibronic sub-band E_{00} of the highest occupied molecular orbital (HOMO) to the lowest molecular orbital (LUMO) for the thin DIP layer [23]. During the experiment, the laser output power was adjusted to 2.5 mW to avoid molecular photobleaching. The beam spot size at the sample surface was ~ 1 mm to excite a sufficiently large area and circumvent detecting possible spatial inhomogeneities of the grown organic layer. The incoming laser beam causes the molecular excitation and the subsequent PL signal is detected in the central port (in the middle of the chamber top, see Fig. 1b). The PL signal is collected by a vacuum-compatible achromatic doublet lens. The second achromatic lens doublet of infinity conjugated pair focuses the PL signal into the multimode optical fiber with a core diameter of 900 μm (Witec). Finally, the optical fiber is connected to a spectrometer (grating 150 g/mm, Acton SpectraPro), equipped with a thermoelectrically cooled CCD camera (iDus 420BU, Andor). Two longpass filters with a cut-off wavelength of 550 nm were placed in front of the optical fiber to suppress the excitation laser entering the spectrophotometer.

For the actual molecular deposition, the chamber was pumped by a turbomolecular pump, which was connected to a standard flange in the lower part of the chamber (below the sample holder). The base pressure

was on the order of 10^{-8} mbar. The molecules were grown on a native oxide silicon wafer that was annealed at 120 °C before the deposition to avoid surface contamination and then cooled down to a steady temperature of 50 °C. Finally, the DIP cell was heated to 255 °C, yielding an evaporation rate of ~ 2.5 $\text{\AA}/\text{min}$. The deposition rate was monitored in real time with a quartz crystal microbalance (QCM). As generally known, DIP molecules exhibit a well-defined layer-plus-islands growth mode (Stranski-Krastanov) with an almost upright molecular orientation [22,25], so the deposition rate is inferred from the *effective* layer thickness obtained from the *ex-situ* ellipsometry measurements [23].

For GIWAXS measurement, we used a custom-made laboratory system consisting of a MetalJet X-ray source (Excillum) with an X-ray energy of 9.25 keV ($\lambda = 1.34$ \AA). The total X-ray flux was $\sim 10^8$ photons/s on the sample area of ~ 10 mm², which is below the damage threshold of the DIP film. The incidence angle of the incoming X-ray beam (α_i) was set to 0.2°. The GIWAXS diffraction patterns were collected by a hybrid-pixel two-dimensional detector (Pilatus 300 K, Dectris) with a 320 μm thick Si sensor.

3. Results and discussion

DIP is an organic fluorescent material [27,28] with an absorption edge around ~ 2.1 eV for a thin film, followed by a vibronic progression [20,23,29]. We excited the sample by a 532 nm laser (~ 2.3 eV) from the very beginning of DIP growth, and the PL signal was measured. Fig. 2 shows the normalized PL spectra obtained *in situ* during the deposition of DIP molecules for several selected effective thicknesses of the grown layer. The PL signal represents the electron relaxation from LUMO to HOMO (rigorously referred to as fluorescence from $S_1 \rightarrow S_0$) in an ensemble of excited DIP molecules. At least two peaks are clearly distinguishable (for layers thicker than 0.2 nm) from the PL spectra, corresponding to C–C vibrational modes that are typical of conjugated molecules [30]. The first peak in the PL spectrum is located at $E_{00} \sim 2.15$ eV – for a layer thicker than 2 nm – with the vibronic progression of

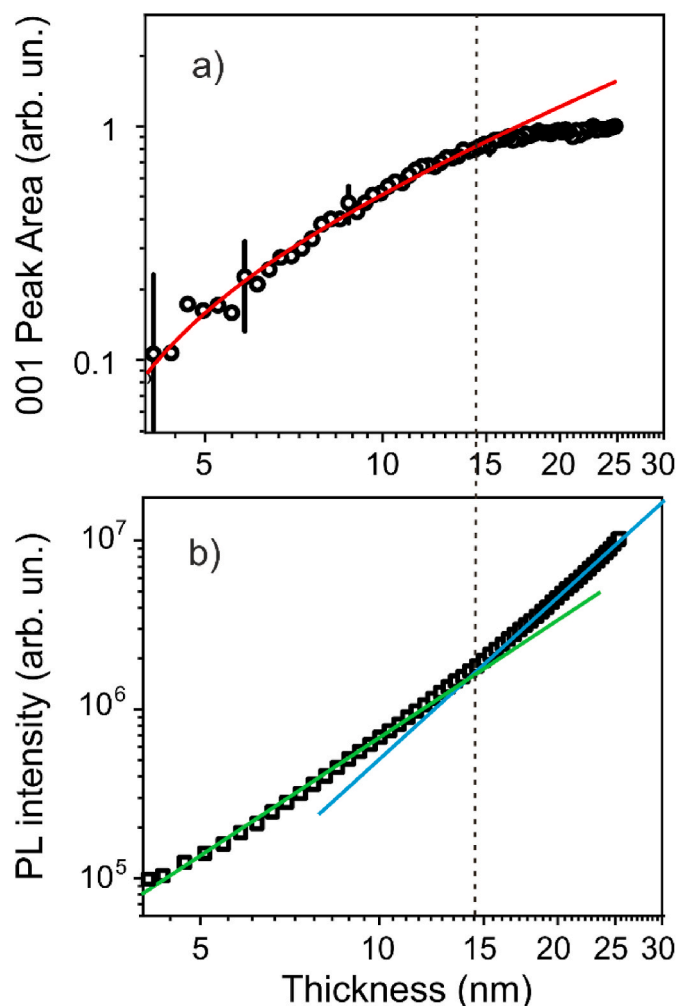


Fig. 5. Thickness dependence of the a) normalized scattering intensity of the 001 diffraction peak and b) overall PL intensity. The red line in a) is a linear fit of the diffraction peak intensity in the first half of the molecular growth. The green and blue lines in b) represent a PL intensity fit in the first and second halves of the molecular growth, respectively. (For interpretation of the references to colour in this figure legend, the reader is referred to the Web version of this article.)

$\Delta E = (0.16 \pm 0.01)$ eV. The Stokes shift calculated from the lowest vibronic subband in the absorption spectrum of the DIP thin film, is ~ 0.11 eV, which is in good agreement with previous reports [20,28].

The measured emission energy distribution (spectral shape) given by the molecular interaction changes significantly with the layer thickness. At the beginning of the growth, the first vibronic peak is the most intense one, indicating the presence of non-interacting molecules on the Si substrate, similar to various small organic molecules in the solution [19, 20,31–33]. On the other hand, with an increasing amount of evaporated molecules and thus the effective layer thickness, the interaction between the molecules becomes more pronounced. Thus, the intensity of the first peak diminishes compared to the intensity of the second vibronic peak. The interaction-induced changes in the vibronic intensity ratios are generally of key importance as they can be exploited to unravel the relationship between the photophysical properties and molecular (or polymer) arrangement [34,35]. In particular, the PL intensity ratios of the first two vibronic peaks ($I_{PL}^{0-0}/I_{PL}^{0-1}$) may provide information regarding an excitation coherence length and a disorder nature (type and amount of defects) [34,36,37]. We note that the position of the PL peaks is redshifting with increasing DIP layer thickness, in agreement with the redshift of the absorption spectrum observed by Hagara et al., [23] due

to the enhanced dielectric screening caused by growing molecular coverage [35]. The overall redshift in the PL spectrum is ~ 50 meV from the onset of the growth up to 15 nm thick layer (the PL spectrum shift is negligible for DIP effective thickness greater than 15 nm). Here, we would like to emphasize that the same energy shift was observed for the 0-0 and 0-1 vibronic peaks. A similar shift in absorption energy (55 meV) was measured by Heinemeyer et al. for pentacene molecules evaporated on native Si substrate [38].

Fig. 3 shows that the overall spectrally integrated PL intensity increases with DIP layer thickness, exhibiting an exponential-like dependency. The increase of the PL intensity is due to the fact that more molecules contribute to the measured signal during the film growth. The non-linear character of the PL intensity increase might be attributed to molecular superradiance caused by a coherent emission of the molecular ensemble [39]. Other effects, such as quenching at an interface, might also be at work so that the resulting thickness dependence would be non-linear. A similar character of the overall PL intensity thickness dependence was observed by Müller et al. [40] for rubrene molecules on AlO_x . Apparently, the PL intensity should saturate at a certain thickness due to a limited penetration depth of the excitation laser. Based on the known absorption coefficient of DIP, such a penetration depth should be around 100–200 nm [41,42]. However, in our case, the grown DIP layers were much thinner, so we did not observe any saturation of the PL signal.

The overall aim of the presented experimental setup was to correlate the PL properties with the structural ones. Thus, we now turn to the GIWAXS results. Fig. 4 shows the GIWAXS reciprocal space maps of the 5 nm and 25 nm thick DIP film. A Bragg diffraction spot is visible at $q_{\perp} \approx 0.39 \text{ \AA}^{-1}$ for both thicknesses, corresponding to reflection from (001) lattice planes. The 001 diffraction along q_{\perp} indicates a standing-up orientation of the molecules [22,23,43]. Similarly, the standing-up molecular orientation can be deduced from the wedding-cake-like growth of the DIP crystals measured by AFM (see Fig. 4c), which is typical for the upright orientation of the DIP molecules on Si substrates [22,27]. A slight shift in the Bragg peak position from $q = (0.360 \pm 0.005) \text{ \AA}^{-1}$ for 5 nm to $q = (0.390 \pm 0.005) \text{ \AA}^{-1}$ for the 25 nm thick film can be observed in Fig. 4. The peak position was calculated by fitting the linecuts in the reciprocal space map with a Gaussian function. For clarity, in laboratory conditions where the intensity of the X-ray source is limited, the position (and intensity) of the diffraction peak can be reliably determined from ~ 4 nm. For thinner DIP layers, the background scattering hinders measuring the diffraction peak intensity. A similar peak shift during the DIP growth was observed previously [44] and attributed to structural changes, i.e., a change of lattice parameters induced by strain or inhomogeneities.

As expected, the scattering intensity increases with DIP thickness [45]. However, the intensity increase is not linear, as can be seen from the deviation of the experimental data from the linear function, plotted as a red curve in Fig. 5a. We note that the scattering intensity shown in Fig. 5a was calculated as the peak area and normalized to its maximal value. The log-log scale was intentionally chosen to directly compare with the PL intensity, as explained in the following paragraph.

The scattering intensity rises linearly up to ~ 14 nm, and its growth slows down subsequently. In ideal layer-by-layer growth, the intensity of the diffraction peaks is expected to scale linearly with the film thickness. A lower rate in the intensity increase might indicate an existence of a competing polymorph. In earlier work, Kowarik et al. [25,44] observed the formation of a new polymorph characterized by *lying-down* molecular orientation starting at a critical thickness of ~ 17 nm (at a substrate temperature of $35 \text{ }^{\circ}\text{C}$). Interestingly, the PL intensity evolution also shows a non-linear thickness dependence when plotted on the logarithmic scale (Fig. 5b). Here, two growth regions can be distinguished based on the distinct linear slope: (1) and early-stage growth, from ~ 4 to 14 nm, and (2) from ~ 14 to 25 nm. In both regions, the PL intensity scales approximately linearly (linear in the log-log scale, i.e., exponential in the linear scale) with the film thickness, albeit with a different

scaling factor. We note that the PL intensity thickness dependence was measured several times, and its deviation from the linear trend (on a logarithmic scale) is reproducible.

The PL signal is very sensitive to the transition dipole moment of the molecule μ , i.e., to the molecular orientation [17,46]. The DIP molecule is known to have μ parallel to the long molecular axis [29,47]. For the standing-up direction of DIP, the projection of incident electric field E and μ is smaller compared to the case of lying-down molecules [23]. Thus, in addition to the increasing number of luminescent molecules, the increase in the PL intensity could potentially be explained by concurrent growth of two molecular orientations –standing-up and lying-down. On the other hand, the lying-down molecular orientation was not observed in our GIWAXS measurements. For the lying-down molecules, the diffraction peak would appear near $q_{||} \approx 0.39 \text{ \AA}^{-1}$ as indicated by the red square in Fig. 4b. However, the 001 diffraction intensity for the lying-down molecules is generally less pronounced compared to the standing-up orientation, as the lying-down molecules are typically oriented in the so-called fiber texture (arbitrary azimuthal orientation) [48]. In this case, the diffraction would also realize at all azimuthal angles above the sample plane, reducing the intensity of the 001 diffraction. Moreover, the volume of the lying-down molecular phase might be too small to be clearly distinguishable from the background scattering. Therefore, an X-ray source with higher photon flux, such as synchrotron radiation, would be required to confirm the existence of the lying-down molecular orientation directly.

4. Conclusion

In conclusion, we present simultaneous *in situ* X-ray diffraction and photoluminescence measurements during molecular growth in a vacuum. We found a direct correlation between the PL and GIWAXS diffraction intensities, indicating the formation of a new polymorph with a lying-down orientation of DIP molecules starting at a layer thickness of ~ 14 nm. We show that, as expected, the PL signal is more sensitive to the arrangement of the molecules than the GIWAXS. Furthermore, we emphasize that the presented deposition chamber with PL add-on can be widely used not only for studying the real-time growth of molecular layers but also the growth of vacuum-deposited perovskites and other photoluminescent materials, where the correlation of electronic and structural properties is of high importance.

Declaration of competing interest

The authors declare that they have no known competing financial interests or personal relationships that could have appeared to influence the work reported in this paper.

Acknowledgments

We would like to acknowledge the financial support of the following grants: APVV-17-0352, APVV-19-0465, SK-CN-RD-18-0006, SK-AT-20-0006, APVV-20-0111, APVV-14-0120, VEGA 2/0059/21, VEGA 2/0041/21, VEGA 2/0046/21, ITMS 313011U400, DAAD/SAV, and the funding by the DFG. This work was performed during the implementation of the project Building-up Centre for Advanced Materials Application of the Slovak Academy of Sciences, ITMS project code 313021T081, supported by the Research & Innovation Operational Programme funded by the ERDF.

References

- [1] Y.L. Shi, X.D. Wang, *Adv. Funct. Mater.* 31 (2021) 2008149.
- [2] Y. Yu, Y.C. Tao, S.N. Zou, Z.Z. Li, C.C. Yan, M.P. Zhuo, X.D. Wang, L.S. Liao, *Sci. China Chem.* 63 (2020) 1477.
- [3] M.-P. Zhuo, Y. Yuan, Y. Su, S. Chen, Y.T. Chen, Z.Q. Feng, Y.K. Qu, M.D. Li, Y. Li, B. W. Hu, X.D. Wang, L.S. Liao, *Adv. Mater.* 34 (2022) 2107169.
- [4] J.J. Wu, M.P. Zhuo, R. Lai, S.N. Zou, C.C. Yan, Y. Yuan, S.Y. Yang, G.Q. Wei, X. D. Wang, L.S. Liao, *Angew. Chem. Int. Ed.* 60 (2021) 9114.
- [5] M.P. Zhuo, Y. Su, Y.K. Qu, S. Chen, G.P. He, Y. Yuan, H. Liu, Y.C. Tao, X.D. Wang, L.S. Liao, *Adv. Mater.* 33 (2021) 2102719.
- [6] M.P. Zhuo, G.P. He, Y. Yuan, Y.C. Tao, G.Q. Wei, X.D. Wang, S.T. Lee, L.S. Liao, *CCS Chem.* 3 (2021) 413.
- [7] T. Michely, J. Krug, *Islands and Atoms*, Springer, 2004.
- [8] M. Einax, W. Dieterich, P. Maass, *Rev. Mod. Phys.* 85 (2013) 921.
- [9] S. Bommel, N. Kleppmann, C. Weber, H. Spranger, P. Schäfer, J. Novak, S.V. Roth, F. Schreiber, S.H.L. Klapp, S. Kowarik, *Nat. Commun.* 5 (2014) 1.
- [10] J. Yang, S. Yim, T.S. Jones, *Sci. Rep.* 5 (2015) 1.
- [11] K. Suchan, J. Just, P. Becker, E.L. Unger, T. Unold, *J. Mater. Chem. A* 8 (2020) 10439.
- [12] J. Schlipf, P. Müller-Buschbaum, *Adv. Energy Mater.* 7 (2017) 1.
- [13] L. Qu, X. Peng, *J. Am. Chem. Soc.* 124 (2002) 2049.
- [14] S. Kowarik, A. Gerlach, F. Schreiber, *J. Phys. Condens. Matter* 20 (2008) 184005.
- [15] N. Mrkyvkova, P. Nadazdy, M. Hodas, J. Chai, S. Wang, D. Chi, M. Sojkova, M. Hulman, A. Chumakov, O.V. Konovalov, A. Hinderhofer, M. Jergel, E. Majkova, P. Siffalovic, F. Schreiber, *Cryst. Growth Des.* 20 (2020) 5269.
- [16] S. Kowarik, A. Gerlach, S. Sellner, L. Cavalcanti, O. Konovalov, F. Schreiber, *Appl. Phys. Mater. Sci. Process* 95 (2009) 233.
- [17] R. Zimmerleiter, M. Hohage, L. Sun, *Phys. Rev. Mater.* 3 (2019) 83402.
- [18] M. Müller, A. Langner, O. Krylova, E. Le Moal, M. Sokolowski, *Appl. Phys. B Laser Opt.* 105 (2011) 67.
- [19] A. Brillante, T. Salzillo, R.G. Della Valle, E. Venuti, F. Borgatti, E. Lunedei, F. Liscio, S. Milita, C. Albonetti, *J. Lumin.* 187 (2017) 403.
- [20] V.M. Nichols, K. Broch, F. Schreiber, C.J. Bardeen, *J. Phys. Chem. C* 119 (2015) 12856.
- [21] C. Schuenemann, A. Petrich, R. Schulze, D. Wynands, J. Meiss, M.P. Hein, J. Jankowski, C. Elschner, J. Alex, M. Hummert, K.J. Eichhorn, K. Leo, M. Riede, *Org. Electron.* 14 (2013) 1704.
- [22] A.C. Dürr, F. Schreiber, M. Münch, N. Karl, B. Krause, V. Kruppa, H. Dosch, *Appl. Phys. Lett.* 81 (2002) 2276.
- [23] J. Hagara, N. Mrkyvkova, P. Nadazdy, M. Hodas, M. Bodík, M. Jergel, E. Majkova, K. Tokár, P. Hutár, M. Sojkova, A. Chumakov, O. Konovalov, P. Pandit, S. Roth, A. Hinderhofer, M. Hulman, P. Siffalovic, F. Schreiber, *Phys. Chem. Chem. Phys.* 22 (2020) 3097.
- [24] K.A. Ritley, B. Krause, F. Schreiber, H. Dosch, *Rev. Sci. Instrum.* 72 (2001) 1453.
- [25] S. Kowarik, A. Gerlach, F. Schreiber, *J. Phys. Condens. Matter* 20 (2008) 184005.
- [26] M. Heilig, M. Domhan, H. Port, *J. Lumin.* 110 (2004) 290.
- [27] D. Zhang, A. Horneber, J. Mihaljevic, U. Heinemeyer, K. Braun, F. Schreiber, R. Scholz, A.J. Meixner, *J. Lumin.* 131 (2011) 50.
- [28] U. Heinemeyer, R. Scholz, L. Gisslén, M.I. Alonso, J.O. Ossó, M. Garriga, A. Hinderhofer, M. Kytka, S. Kowarik, A. Gerlach, F. Schreiber, *Phys. Rev. B* 78 (2008) 85210.
- [29] M. Pope, C.E. Swenberg, *Electronic Processes in Organic Crystals and Polymers*, Oxford University Press, 1999.
- [30] M.A. Loi, E.D.A. Como, F. Dinelli, M. Murgia, R. Zamboni, F. Biscarini, M. Muccini, *Nat. Mater.* 4 (2005) 81.
- [31] A.D. Platt, J. Day, S. Subramanian, J.E. Anthony, O. Ostroverkhova, *J. Phys. Chem. C* 113 (2009) 14006.
- [32] B. Valeur, M.N. Berberan-Santos, *Molecular Fluorescence: Principles and Applications*, Wiley-VCH Verlag & Co., 2012.
- [33] F.C. Spano, C. Silva, *Annu. Rev. Phys. Chem.* 65 (2014) 477.
- [34] U. Heinemeyer, K. Broch, A. Hinderhofer, M. Kytka, R. Scholz, A. Gerlach, F. Schreiber, *Phys. Rev. Lett.* 104 (2010) 257401.
- [35] F.C. Spano, *J. Chem. Phys.* 116 (2002) 5877.
- [36] F. Otieno, L. Kotane, M. Airo, C. Billing, R.M. Erasmus, D. Wamwangi, D.G. Billing, *Eur. Phys. J. Plus* 136 (2021).
- [37] U. Heinemeyer, K. Broch, A. Hinderhofer, M. Kytka, R. Scholz, A. Gerlach, F. Schreiber, *Phys. Rev. Lett.* 104 (2010) 257401.
- [38] J.C. MacGillivray, M.S. Feld, *Contemp. Phys.* 22 (1981) 299.
- [39] M. Müller, A. Langner, O. Krylova, E. Le Moal, M. Sokolowski, *Appl. Phys. B Laser Opt.* 105 (2011) 67.
- [40] D. Greiner, V. Hinrichs, S. Wiesner, W. Ludwig, K. Fostiropoulos, D. Keiper, P. K. Baumann, N. Meyer, M. Heuken, M. Rusu, M.C. Lux-Steiner, *Thin Solid Films* 534 (2013) 255.
- [41] U. Wurfel, M. Thorwart, E.R. Weber, *Quantum Efficiency in Complex Systems, Part II: from Molecular Aggregates to Organic Solar Cells*, Academic Press, 2011.
- [42] X.N. Zhang, E. Barrena, D. Garcia De Oteyza, E. De Souza, H. Dosch, *J. Appl. Phys.* 104 (2008) 2.
- [43] S. Kowarik, A. Gerlach, S. Sellner, F. Schreiber, L. Cavalcanti, O. Konovalov, *Phys. Rev. Lett.* 96 (2006) 125504.
- [44] K.D. Bowen, B.K. Tanner, *High Resolution X-Ray Diffractometry and Topography*, CRC Press, London, 1998.
- [45] J. Frischeisen, D. Yokoyama, C. Adachi, W. Brütting, *Appl. Phys. Lett.* 96 (2010) 73302.
- [46] C. Schünemann, D. Wynands, K.J. Eichhorn, M. Stamm, K. Leo, M. Riede, *J. Phys. Chem. C* 117 (2013) 11600.
- [47] N. Mrkyvkova, M. Hodas, J. Hagara, P. Nadazdy, J. Halahovetz, M. Bodík, K. Tokár, J.W. Chai, S.J. Wang, D.Z. Chi, A. Chumakov, O. Konovalov, A. Hinderhofer, M. Jergel, E. Majkova, P. Siffalovic, F. Schreiber, *Appl. Phys. Lett.* 114 (2019) 251906.